

Systematic Variation of Metal–Metal Bond Order in Metal–Chromium Complexes[†]

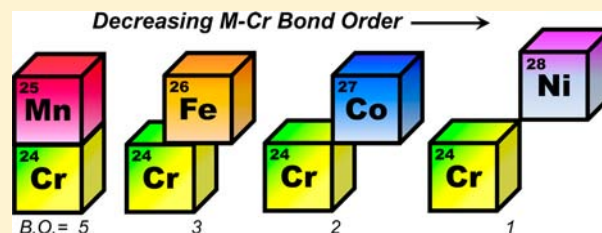
Laura J. Clouston,^{‡,||} Randall B. Siedschlag,^{‡,||} P. Alex Rudd,[‡] Nora Planas,^{‡,§} Shuxian Hu,^{‡,§} Adam D. Miller,[‡] Laura Gagliardi,^{‡,§} and Connie C. Lu^{*,‡}

[‡]Department of Chemistry, University of Minnesota, 207 Pleasant Street SE, Minneapolis, Minnesota 55455-0431, United States

[§]Supercomputing Institute, and Chemical Theory Center, University of Minnesota, Minneapolis, Minnesota 55455, United States

S Supporting Information

ABSTRACT: In the field of metal–metal bonding, the occurrence of stable, multiple bonds between different transition metals is uncommon, and is largely unknown for different first-row metals. Adding to a recently reported iron–chromium complex, three additional M–Cr complexes have been isolated, where the iron site is systematically replaced with other first-row transition metals (Mn, Co, or Ni), while the chromium site is kept invariant. These complexes have been characterized by X-ray crystallography. The Mn–Cr complex has an ultrashort metal–metal bond distance of 1.82 Å, which is consistent with a quintuple bond. The M–Cr bond distances increases across the period from M = Mn to M = Ni, as the formal bond order decreases from 5 to 1. Theoretical calculations reveal that the M–Cr bonds become increasingly polarized across the period. We propose that these trends arise from increasing differences in the energies and/or contraction of the metals' d-orbitals (M vs Cr). The cyclic voltammograms of these heterobimetallic complexes show multiple one-electron transfer processes, from two to four redox events depending on the M–Cr pair.



The M–Cr bond distances increases across the period from M = Mn to M = Ni, as the formal bond order decreases from 5 to 1. Theoretical calculations reveal that the M–Cr bonds become increasingly polarized across the period. We propose that these trends arise from increasing differences in the energies and/or contraction of the metals' d-orbitals (M vs Cr). The cyclic voltammograms of these heterobimetallic complexes show multiple one-electron transfer processes, from two to four redox events depending on the M–Cr pair.

INTRODUCTION

Multiple bonds between metal atoms have intrigued chemists for over 50 years.^{1,2} Our understanding of these unusual bonds has been marked by several key discoveries. In 1964, Cotton and co-workers elucidated the quadruple bond in the dirhenium complex, [Re₂Cl₈]²⁻, which ushered in a boom of multiply bonded metal–metal compounds.^{3–5} In 2005, Power and co-workers reported the first quintuple bond in a dichromium complex.⁶ Chemists began anew to make molecules with ultrashort metal–metal bonds^{7–10} and to understand their bonding theoretically.^{11–14}

In contrast, far less is known about multiple bonds between different metals.^{15–18} Given the vast possibilities of metal–metal bonds that can potentially be formed from the d-block elements, it is likely that unprecedented chemical bonding and/or properties will emerge. Unfortunately, very few species of this type have been isolated. To our knowledge, the largest family of heterometallic M–M' multiple bonds are the (por)MM'(por) complexes prepared by Collman and co-workers, where M = (Mo, W), M' = (Re, Ru, Os), and por = porphyrin.^{15,19} These heterodinuclear cores were assembled by pyrolyzing the mononuclear metalloporphyrin precursors. Notably, the authors did not observe any metal–metal bond formation with any first-row metalloporphyrins.

Indeed, bonds between first-row metals are generally weaker than those of their heavier congeners, presumably because of the poor overlap between the smaller 3d orbitals. Some of the early successes in preparing heterodinuclear cores of first-row metals were achieved using argon matrices at low temper-

atures.^{20,21} These bimetallic species are bare, or unligated. Interestingly, several of them exhibited high vibrational frequencies, suggesting multiple bond character.^{22,23} However, their transient nature made it challenging to conduct reactivity studies. Recently, two coordination examples demonstrate that auxiliary ligands can stabilize heterometallic multiple bonds of first-row transition metals.^{24,25} These compounds feature ultrashort bonds between iron and chromium, and iron and vanadium. They share a trigonal coordination environment, with amides binding to the chromium or vanadium centers, and with phosphines coordinating the iron center. Remarkably, for a variety of d-electron counts, ranging from d⁹ in [FeV]⁴⁺ to d¹² in [FeCr]²⁺, the metal pairs remain multiply bonded. Their isolation thus opens a new horizon in the vista of metal–metal bonding.

We report an isostructural, four-membered series of first-row M–Cr heterobimetallics, for M = Mn (1),²⁶ Fe (2),^{27,28} Co (3), and Ni (4), and their electronic structures. With this family, we demonstrate that metal–chromium bonds can be systematically tuned by varying the metal identity. Moreover, these metal–chromium bonds reveal rich redox profiles, which may be useful in reactivity.^{29,30} With this series in hand, we have a unique opportunity to evaluate periodic trends in their bonding nature as well as their electrochemical properties.

Received: June 26, 2013

Published: July 31, 2013

Table 1. Crystallographic Details for Complexes 1, 3, 4, and 5

	1	3	4	5
chemical formula	C ₃₉ H ₆₀ CrMnN ₄ P ₃	C ₃₉ H ₆₀ CoCrN ₄ P ₃	C ₃₉ H ₆₀ N ₄ CrNiP ₃ ·0.5(O(CH ₂ CH ₃) ₂)	C ₃₉ H ₆₃ N ₄ NiP ₃ ·0.5(C ₇ H ₈)
fw	784.76	788.75	825.62	785.62
cryst syst	trigonal	triclinic	triclinic	triclinic
space group	P321	P $\bar{1}$	P $\bar{1}$	P $\bar{1}$
a (Å)	15.979(2)	12.371(2)	11.121(2)	11.373(1)
b (Å)	15.979(2)	19.416(3)	14.167(2)	14.050(1)
c (Å)	11.692(1)	19.653(3)	14.256(2)	14.181(1)
α (deg)	90	113.252(2)	71.694(2)	71.846(1)
β (deg)	90	95.561(2)	83.745(2)	80.484(1)
γ (deg)	120	101.549(2)	81.854(2)	82.265(1)
V (Å ³)	2585.1(5)	4167.5(1)	2105.9(5)	2115.3(3)
Z	2	4	2	2
D _{calcd} (g cm ⁻³)	1.008	1.257	1.302	1.233
λ (Å), μ (mm ⁻¹)	0.710 73, 0.572	0.710 73, 0.805	0.710 73, 0.853	0.710 73, 0.606
T (K)	173(2)	173(2)	173(2)	173(2)
θ range (deg)	2.28–27.42	1.87–25.04	1.51–27.52	1.52–27.50
reflns collected	12 767	34 306	24 583	24 513
unique reflns	3040	7633	6867	7339
data/restraint/params	3922/0/149	14 553/0/889	9577/4/490	9566/11/465
R1, wR2 (I > 2 σ (I))	0.0472, 0.1129	0.0606, 0.1160	0.0592, 0.1611	0.0450, 0.1120

EXPERIMENTAL SECTION

General Considerations. Unless otherwise stated, all manipulations were performed under a dinitrogen atmosphere in an MBraun or VAC glovebox or using standard Schlenk techniques. Standard solvents were deoxygenated by sparging with dinitrogen and dried by passing through activated alumina columns of a SG Water solvent purification system. Deuterated solvents were purchased from Cambridge Isotope Laboratories, Inc., degassed via freeze–pump–thaw cycles, and stored over activated 4 Å molecular sieves. ¹H NMR spectra were recorded on Varian 300 MHz or a Bruker 500 MHz spectrometer at ambient temperature unless otherwise stated. Elemental analyses were performed by Complete Analysis Laboratories, Inc. (Parsippany, NJ). Cyclic voltammetry was conducted using a CH Instruments 600 electrochemical analyzer. The one-cell setup utilized a glassy carbon working electrode, platinum wire counter electrode, and Ag/AgNO₃ reference electrode in acetonitrile. Analyte solutions were prepared in a THF solution of tetra-n-butylammonium hexafluorophosphate (0.1 M) and referenced internally to the FeCp₂/FeCp₂⁺ redox couple. The monometallic chromium complex, Cr(N(o-(NCH₂PⁱPr₂)C₆H₄)₃), and the iron–chromium complex, FeCr(N(o-(NCH₂PⁱPr₂)C₆H₄)₃), were prepared according to literature procedures.²⁴ Magnetic susceptibility data were measured from powder samples of solid material in the temperature range 2–300 K by using a SQUID susceptometer with a field of 1.0 T (MPMS-7, Quantum Design, calibrated with standard palladium reference sample, error < 2%). The experimental data were corrected for underlying diamagnetism by use of tabulated Pascal's constants.³¹ The susceptibility and magnetization data were simulated with the program jux.³²

Synthesis of 1, MnCr(N(o-(NCH₂PⁱPr₂)C₆H₄)₃). A solution of Cr(N(o-(NCH₂PⁱPr₂)C₆H₄)₃) (0.200 g, 0.275 mmol) was dissolved in THF (ca. 4 mL) and mixed with a stirred slurry of MnBr₂ (0.036 g, 0.28 mmol) in THF (ca. 4 mL). An inky brown solution formed quickly, and a slurry of K₂C₈ (0.064 g, 0.57 mmol) in THF (ca. 4 mL) was added immediately. Within minutes, a dark red solution formed concomitant with precipitation. The sample was filtered through a Celite plug, which was washed with minimal THF. The solution was dried in vacuo, yielding a maroon powder (0.228 g, 80%). Single crystals of **1** were grown from vapor diffusion of pentane into a concentrated solution of **1** in THF. ¹H NMR (ppm, THF-*d*₈, 500 MHz, –40 °C): 6.65 (t, *J* = 7 Hz, 1H), 6.40 (d, *J* = 7 Hz, 1H), 6.25 (d, *J* = 7 Hz, 1H), 5.88 (t, *J* = 7 Hz, 1H), 5.44 (d, *J* = 13 Hz, 1H), 4.88 (d, *J* = 12 Hz, 1H), 2.94 (br, 1H), 2.75 (br, 1H), 1.75 (overlapping with

THF), 1.46 (br, 3H), 1.35 (br, 3H), 0.50 (br, 3H). ¹³C NMR (ppm, THF-*d*₈, 126 MHz, –40 °C): 155, 135.3, 125.6, 125.5, 110.3, 105.8, 61.9, 29.5, 27.5, 21.7, 19.8, 18.7, 17.7. ³¹P NMR (ppm, THF-*d*₈, 200 MHz): 19.5. UV–vis–NIR (THF) λ_{max} nm (ϵ , M⁻¹ cm⁻¹): 400 (4440), 550 (1850), 1025 (2160). Anal. Calcd for **1** C₃₉H₆₀N₄P₃CrMn: C, 59.69; H, 7.71; N, 7.14. Found: C, 59.63; H, 7.84; N, 7.22.

Synthesis of 3, CoCr(N(o-(NCH₂PⁱPr₂)C₆H₄)₃). A solution of Cr(N(o-(NCH₂PⁱPr₂)C₆H₄)₃) (0.302 g, 0.414 mmol) was dissolved in THF (ca. 4 mL) and added to a slurry of CoBr₂ (0.091 g, 0.42 mmol) in THF (ca. 4 mL). After stirring the dark green brown solution for 1 h, a slurry of K₂C₈ (0.115 g, 0.852 mmol) in THF was added. After stirring for an additional hour, the solution was then filtered through a Celite pad, which was washed with THF until the washings were clear. The solution was dried in vacuo to give a brown powder (0.310 g, 95% yield). Single crystals were grown from vapor diffusion of pentane into a concentrated solution of **3** in THF. ¹H NMR (ppm, THF-*d*₈, 500 MHz): 10.5, 6.1, 2.4, 0.7, –1.0, –4.8. Evans' method (C₆D₆): $\mu_{\text{eff}} = 2.76 \mu_{\text{B}}$. UV–vis–NIR (THF) λ_{max} nm (ϵ , M⁻¹ cm⁻¹): 325 sh (24 000), 440 sh (4400), 520 sh (2600), 840 sh (650), 1420 (950). Anal. Calcd for **3** C₃₉H₆₀N₄P₃CrCo: 59.39 C, 7.67 H, 7.10 N. Found: 59.31 C, 7.73 H, 7.06 N.

Synthesis of 4, NiCr(N(o-(NCH₂PⁱPr₂)C₆H₄)₃). A solution of Cr(N(o-(NCH₂PⁱPr₂)C₆H₄)₃) (0.110 g, 0.152 mmol) in THF (10 mL) was added to Ni(COD)₂ (where COD = 1,5-cyclooctadiene) (0.042 g, 0.15 mmol) and stirred at rt for 1 h, during which the color changed from brown-yellow to brown-red. The solvent was then removed in vacuo. The residue was then dissolved in toluene and filtered through a Celite pad. The solvent was removed in vacuo overnight to yield a brown powder **3** (0.1161 g, 97% yield). Single crystals suitable for X-ray diffraction analysis were grown from vapor diffusion of diethyl ether into a concentrated solution of **4** in toluene. UV–vis–NIR (THF) λ_{max} nm (ϵ , M⁻¹ cm⁻¹): 325 sh (24 000), 429 sh (6300), 568 (1900), 934 (110). Evans' Method (C₆D₆): $\mu_{\text{eff}} = 3.80 \mu_{\text{B}}$. ¹H NMR (300 MHz, C₆D₆, ppm): 17.1, 4.5, –15.2. Anal. Calcd for **4** C₃₉H₆₀N₄P₃CrNi: C, 59.40; H, 7.67; N, 7.11. Found: C, 59.37; H, 7.61; N, 6.97.

Synthesis of 5, Ni(N(o-(NHCH₂PⁱPr₂)C₆H₄)₃). To a solution of ligand N(o-(NHCH₂PⁱPr₂)C₆H₄)₃ (48.5 mg, 0.0713 mmol) in THF (ca. 6 mL) was added a stirring slurry of Ni(COD)₂ (19.0 mg, 0.0691 mmol) in THF (ca. 4 mL) dropwise. The solution, which turned to a deep magenta, was stirred for 4 h. The solution was filtered through a Celite pad, and the solvent was removed in vacuo. The resulting solid was washed with cold pentane to yield a magenta powder (50.2 mg, 95%

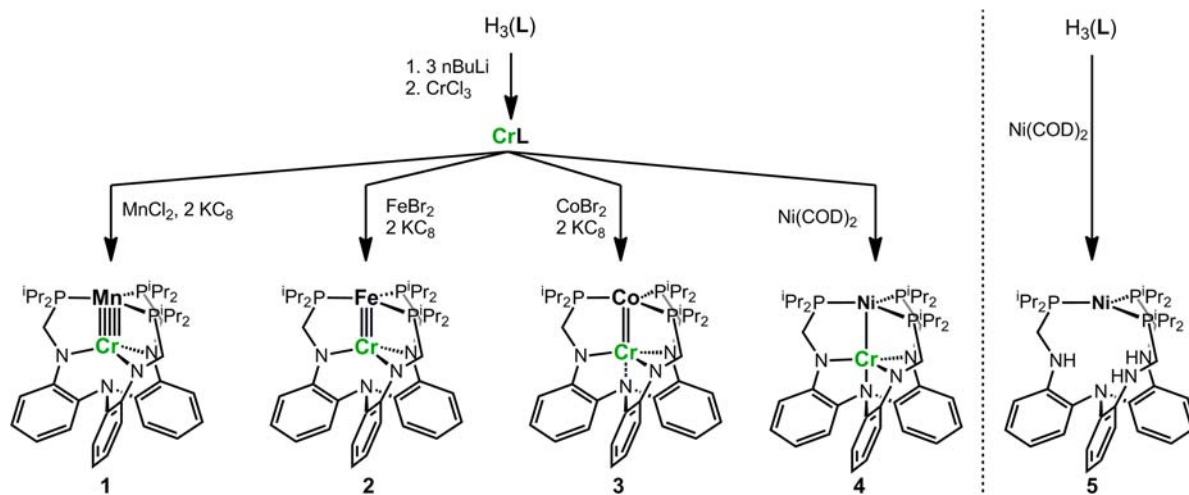


Figure 1. Synthesis of the M–Cr family 1–4 and the monometallic Ni complex, 5. The M–Cr bond varies from formally quintuple to single in this series.

yield). Single crystals suitable for X-ray diffraction were grown from the slow evaporation of diethyl ether. ^1H NMR (ppm, THF- d_8 , 500 MHz): 6.91 (m, 2H), 6.51 (d, $J = 7.7$ Hz, 1H), 6.46 (t, $J = 7.5$ Hz, 1H), 4.99 (s, 1H), 3.27 (s, 2H), 2.10 (br, 2H), 0.78 (m, 12H). ^{13}C NMR (ppm, THF- d_8 , 126 MHz): 145.9, 133.3, 126.9, 126.5, 116.6, 110.6, 49.3, 34.2, 28.3, 23.7, 20.0, 18.1. ^{31}P NMR (ppm, C_6D_6 , 200 MHz): 30.2. Anal. Calcd for 5 $\text{C}_{39}\text{H}_{63}\text{N}_4\text{P}_3\text{Ni}$: C, 63.34; H, 8.59; N, 7.58. Found: C, 63.33; H, 8.64; N, 7.46.

X-ray Crystallographic and Structure Refinement Details. A brown hexagonal plate of 1, a brown block of 3, a brown block of 4, and a red block of 5 were placed onto the tip of a 0.1 mm diameter glass capillary and mounted on a Bruker APEX II CCD diffractometer for data collection at 173(2) K. The data collection was carried out using Mo $K\alpha$ radiation (graphite monochromator). The data intensity was corrected for absorption and decay (SADABS). Final cell constants were obtained from least-squares fits of all measured reflections. The structure was solved using SHELXS-97 and refined using SHELXL-97. A direct-methods solution was calculated which provided most non-hydrogen atoms from the E-map. Full-matrix least-squares/difference Fourier cycles were performed to locate the remaining non-hydrogen atoms. All non-hydrogen atoms were refined with anisotropic displacement parameters. Hydrogen atoms were placed in ideal positions and refined as riding atoms with relative isotropic displacement parameters. Disordered THF solvent molecules were removed from the unit cells of 1 and 3 using Platon SQUEEZE.³³ A disordered THF and toluene molecule residing on an inversion center in the unit cells of 4 and 5, respectively, were each modeled using SHELXTL DFIX and SAME bond distance restraints, and the latter was refined isotropically. Crystallographic data are summarized in Table 1.

COMPUTATIONAL METHODS

DFT Calculations. Gas phase geometry optimizations were performed with DFT using the Perdew–Burke–Ernzerhof (PBE)³⁴ exchange–correlation functional as implemented in the TURBOMOLE 6.4 package.^{35,36} For C and H atoms, the double- ζ quality basis set def-SV(P) was used, whereas the triple- ζ quality basis set def-TZVP was employed for N and P, and additional polarized functions were introduced by using def-TZVPP for Mn, Co, Ni, and Cr. The DFT calculations were performed with the broken symmetry option (unrestricted calculations), and the resolution of the identity (RI) approximation was used for the Coulomb integrals.³⁷ All stationary points were confirmed as minima by vibrational analysis. Initial starting points for geometry optimizations were derived from experimentally determined X-ray structures where the isopropyl groups were replaced with methyls. No symmetry constraints were used.

CASSCF/CASPT2 Calculations. The electronic structure was further investigated using complete active space self-consistent field theory (CASSCF)³⁸ with second-order perturbation theory (CASPT2)^{39,40} on top of the DFT/PBE optimized geometry using the Molcas 7.8 package.⁴¹ Relativistic effects were included through the use of the scalar Douglas–Kroll–Hess (DKH) Hamiltonian.^{42,43} The relativistic all-electron ANO-RCC basis sets^{44,45} were used for all elements. In all of these calculations, the ANO-RCC-VTZP basis set was used for the Ni, Mn, Co, and Cr; ANO-RCC-VDZP basis set was used for N and P; and the ANO-RCC-MB basis set was used for C and H. Additionally, the Cholesky decomposition technique was used combined with local exchange screening to reduce the computational costs involved in generating the two-electron integrals significantly.^{46–48} Atomic charges were computed at the CASSCF level for the ground state using the LoProp procedure.⁴⁹ A complete active space was used consisting of 10 electrons in 15 orbitals, i.e., (10, 15) for 1', a similar active space of (12, 15) was used for 3', and (13, 15) for 4'. The choice of active space was intended to comprise all the valence 3d-electrons and all the 3d orbitals from the two metals and five empty correlating 4d-orbitals of Co, Ni, or Mn.

RESULTS AND DISCUSSION

Synthesis. Previously, we reported the mononuclear chromium and dinuclear iron–chromium (2) coordination complexes of a heptadentate amide–phosphine ligand.^{24,50} To make 2, the chromium and iron were introduced in separate metalation steps.²⁴ This synthetic strategy can be applied to make modular metal–metal bonds by simply varying the metal reagents in either step. As shown in Figure 1, we investigated the pairing of the mononuclear chromium species with different metal precursors to generate a family of metal–chromium complexes, where the metal can be manganese, iron, cobalt, or nickel. In most of these reactions, a metal dihalide reagent was used in tandem with 2 equiv of the reductant KC_8 . For the nickel–chromium compound 4, the labile Ni(0) reagent, $\text{Ni}(\text{COD})_2$ (where COD = 1,5-cyclooctadiene), was preferred because of the ease of removing COD from the product. The heterobimetallic compounds 1–4 were all isolated in good yields (>80%). For comparative purposes, the mononuclear nickel complex 5 was formed by metallating the neutral ligand with $\text{Ni}(\text{COD})_2$.

The manganese–chromium compound 1 is diamagnetic, and its ^1H nuclear magnetic resonance (NMR) spectrum is consistent with three-fold symmetry. Interestingly, the

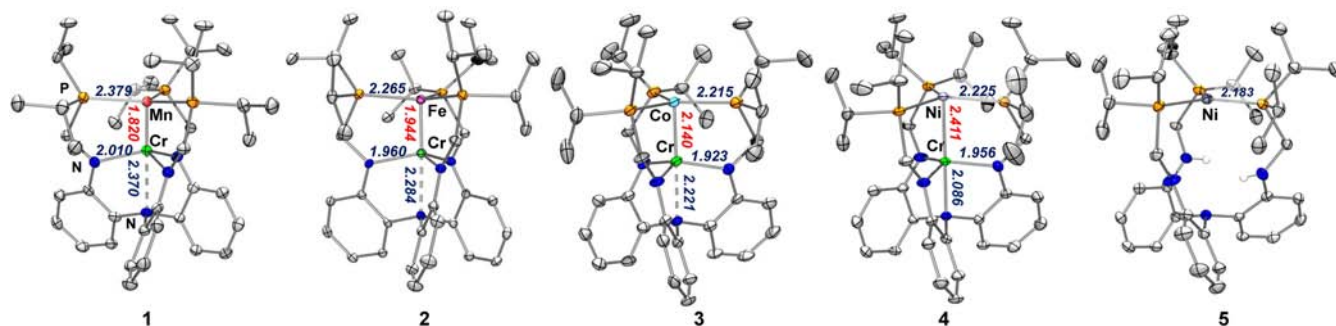


Figure 2. Solid-state structures of the M–Cr family 1–4 and the monometallic Ni complex 5, by X-ray crystallography at 173 K. Thermal ellipsoids are shown at 50% probability. Hydrogen atoms (with the exception of the amine protons in 5) and lattice solvent molecules have been omitted for clarity. Green, chromium; blue, nitrogen; orange, phosphorus; pink, iron; cyan, cobalt; lavender, nickel. M–Cr bond distances are given in red, and average M–P and Cr–N bond distances are given in dark blue.

Table 2. Geometrical Parameters, Including Bond Lengths (Å) and Angles (deg) for Complexes 1–5

	1 MnCr	2 ^a FeCr	3 ^a CoCr	4 NiCr	5 Ni
M–Cr (Å)	1.8192(9)	1.943(1) 1.944(1)	2.135(1) 2.145(1)	2.4105(7)	
r^b	0.78	0.83	0.92	1.04	
M–P (Å)	2.3792(7)	2.265(4) ^c	2.215(5) ^c	2.225(8) ^c	2.183(2) ^c
Cr–N _{eq} (Å)	2.010(3)	1.96(2) ^c	1.923(4) ^c	1.956(9) ^c	
Cr–N _{ap} (Å)	2.370(3)	2.275(3) 2.292(3)	2.216(4) 2.226(4)	2.086(3)	
M to P ₃ -plane (Å)	−0.189	−0.192 ^c	+0.04 ^c	+0.106	+0.033
Cr to N ₃ -plane (Å)	+0.494	+0.412 ^c	+0.372 ^c	+0.276	
∑(P–M–P) (deg)	358.135(6)	357.85(4)	359.89(6)	359.32(4)	359.93(3)
∑(N _{eq} –Cr–N _{eq}) (deg)	342.51(6)	347.1(1)	349.1(2)	354.1(1)	
M–Cr–N _{ap} (deg)	180	176.36(7) 178.71(7)	178.7(1) 179.6(1)	179.46(8)	

^aTwo unique molecules per asymmetric unit. ^b r = ratio of M–Cr bond distance to the sum of M and Cr single-bond metallic radii.⁵⁵ ^cThe average is provided with standard deviation for the average.

methylene protons, which are diastereotopic, resonate downfield at 4.88 and 5.44 ppm. The observed deshielding of these protons is attributed to the diamagnetic anisotropy caused by the circulating electrons within the metal–metal multiple bond.^{51,52} For comparison, the methylene protons of the mononuclear nickel complex 5, which are equivalent, resonate at 3.27 ppm (SI Figure 5). The other bimetallics in this series are paramagnetic. The iron–chromium complex 2 has been previously characterized as an $S = 1/2$ system.²⁴ The magnetic susceptibility plots of 3 and 4 are essentially temperature independent from 40 to 300 K, with values of 3.22 and 3.60 μ_B , respectively (SI Figures 5 and 6). These values are most consistent with $S = 1$ (spin-only magnetic moment, $\mu_{SO} = 2.83 \mu_B$) for cobalt–chromium 3 and an $S = 3/2$ state ($\mu_{SO} = 3.87 \mu_B$) for nickel–chromium 4. Hence, the spin states increase monotonically across the period in the M–Cr series: $S = 0$ for Mn–Cr, $S = 1/2$ for Fe–Cr, $S = 1$ for Co–Cr, and $S = 3/2$ for Ni–Cr.

Solid-State Structures. Single crystal X-ray diffraction studies of complexes 1 and 3–5 provided the solid-state structures shown in Figure 2, with their relevant geometric parameters in Table 2. For comparison, the previously reported compound 2 is also included. All the complexes are essentially three-fold symmetric. The manganese–chromium complex 1 has the shortest metal–metal bond distance in the series, 1.82 Å, which is among the shortest metal–metal bonds ever reported. Ultrashort bonds less than 1.84 Å are otherwise found exclusively in dichromium complexes. Moreover, a search of the Cambridge Structural Database for Mn–Cr bonds shows that previously reported Mn–Cr interactions are weak, at best, with Mn–Cr distances ≥ 2.68 Å.^{53,54}

The solid-state structures of 3 and 4 also reveal short Co–Cr and contracted Ni–Cr bond distances of 2.14 and 2.41 Å, respectively. To better classify the M–Cr bonds across this series, we compare the ratio (r) of the metal–metal bond distance to the sum of the two metals' single-bond radii,⁵⁵ which is identical to Cotton's formal shortness ratio.² The previously reported r value of 0.83 for Fe–Cr 2 was found to be consistent with a triple bond. In comparison, the smaller r value of 0.78 for Mn–Cr 1 suggests an even higher bond order. Meanwhile, the r values of 0.92 for Co–Cr 3 and 1.04 for Ni–Cr 4 indicate double and single bonds, respectively. A clear trend emerges: the M–Cr bond order decreases across the period, i.e., Mn–Cr > Fe–Cr > Co–Cr > Ni–Cr. Indeed, the M–Cr bonding can be systematically tuned over a broad range by a simple swapping of the transition metal element.

It would also be informative to compare the chromium–ligand bond distances in this series. The bond between chromium and the apical nitrogen atom (N_{ap}) decreases steadily from 2.37 Å in 1 to 2.09 Å in 4. This contraction is inversely correlated to the lengthening of the M–Cr bond. The complementary nature of the bonds along the three-fold axis suggests that the position of the chromium atom is sufficiently flexible to accommodate a full range of M–Cr interactions. In contrast, the bonds between chromium and the equatorial nitrogen atoms (N_{eq}) do not change significantly in complexes 2–4 where the overall difference is less than 0.05 Å. Of note, the Cr–N_{eq} and M–P bonds are the longest in 1 compared to the other M–Cr bimetallics.

Electrochemistry. The cyclic voltammograms (CV) have been measured in THF for complexes 1–5, and they are collectively shown in Figure 3. The bimetallics show rich CV

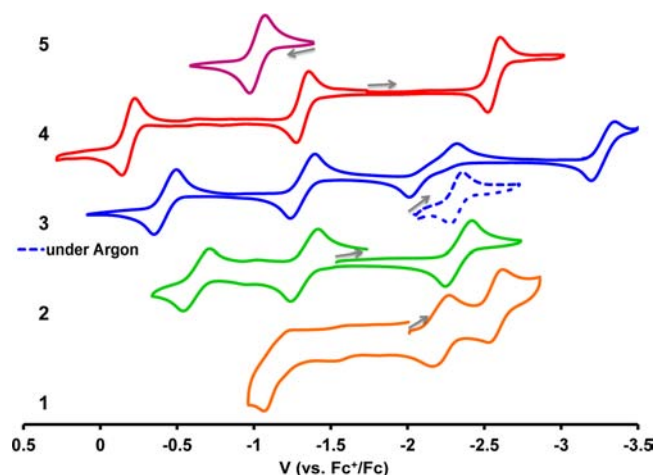


Figure 3. Cyclic voltammograms of 1–5 in 0.1 M or 0.4 M [*n*BuN]PF₆ in THF under N₂ and vs FeCp₂⁺/FeCp₂. In dotted blue, a single scan of 3 under argon. Scan rates for: 1, 250 mV/s; 2, 3, 3 (Ar), 4, 10 mV/s; and 5, 50 mV/s.

profiles composed of two or more reversible and/or quasireversible one-electron-transfer processes. In contrast, mononuclear nickel 5 has a single reversible oxidation at -1.02 V (vs FeCp₂⁺/FeCp₂), which corresponds to a formal Ni(0)/Ni(I) redox couple. The mononuclear chromium precursor has no reversible events in the solvent potential window (SI Figure 7).

Complex 1 has an irreversible oxidation at -1.18 V (SI Figure 8), a reversible reduction at -2.21 V, and a quasireversible reduction at -2.56 V that becomes irreversible at slower scan rates (≤ 100 mV/s, SI Figure 9). The other bimetallics, including Fe–Cr 2, Co–Cr 3, and Ni–Cr 4, each exhibit two reversible oxidative processes. Surprisingly, the redox potentials of the first oxidations are nearly identical at -1.31 to -1.32 V. On the other hand, the second oxidation shifts positively across the period: -0.62 V for Fe–Cr 2, -0.42 V for Co–Cr 3, and -0.18 V for Ni–Cr 4.

Compared to the oxidative processes, the reductive processes vary slightly more in this series. Manganese–chromium 1 and cobalt–chromium 3 each have two reductions, while iron–chromium 2 and nickel–chromium 4 have only one each. Under N₂, the first reduction of 3 appears irreversible by virtue of its large peak potential separation (ΔE_p) of ~ 300 mV. We suspected that dinitrogen binding may ensue upon reduction, inducing a positive shift in the anodic peak. To test this hypothesis, the CV of 3 was measured under argon. The redox potential at -2.32 V becomes reversible under these conditions ($\Delta E_p \sim 79$ mV), validating the hypothesis.

Electron delocalization through the metal–metal bonds would complicate any interpretation of the CV data. Previously, the monoanion of iron–chromium 2 was isolated and found to be consistent with an Fe(0)Cr(II) core by Mössbauer spectroscopy.²⁴ Thus, the reduction event observed at -2.33 V for 2 was attributed to the Cr(III)/Cr(II) redox couple. This redox potential is essentially identical to that observed for cobalt–chromium 3 under argon, suggesting that the latter may also correspond to a chromium-based reduction. Certainly, for the nickel–chromium complex 4, where the d¹⁰ nickel center is incapable of being reduced, it is reasonable that the redox event at -2.56 V is also chromium based. Interestingly, the mononuclear chromium species displays no reductive events, and so its Cr(III)/Cr(II) redox potential is inaccessible within the THF potential window, while the Cr(III)/Cr(II) reduction appears plausible in all the bimetallic complexes of this series. A similar phenomenon, where the reduction of the early metal occurs at a milder potential in the bimetallics versus the monometallic species, has been reported for a related V–Fe system.²⁵

With the exception of 1, the metal–chromium compounds show a reversible oxidative event at nearly identical potentials of -1.32 V (vide infra). It is tempting to interpret this process as a chromium-based oxidation, since chromium is the common element. If the first oxidation can be ascribed to Cr(III)/Cr(IV), then the second oxidation is likely to be centered at the other transition metal, e.g., Fe, Co, or Ni. Specifically for 4, the

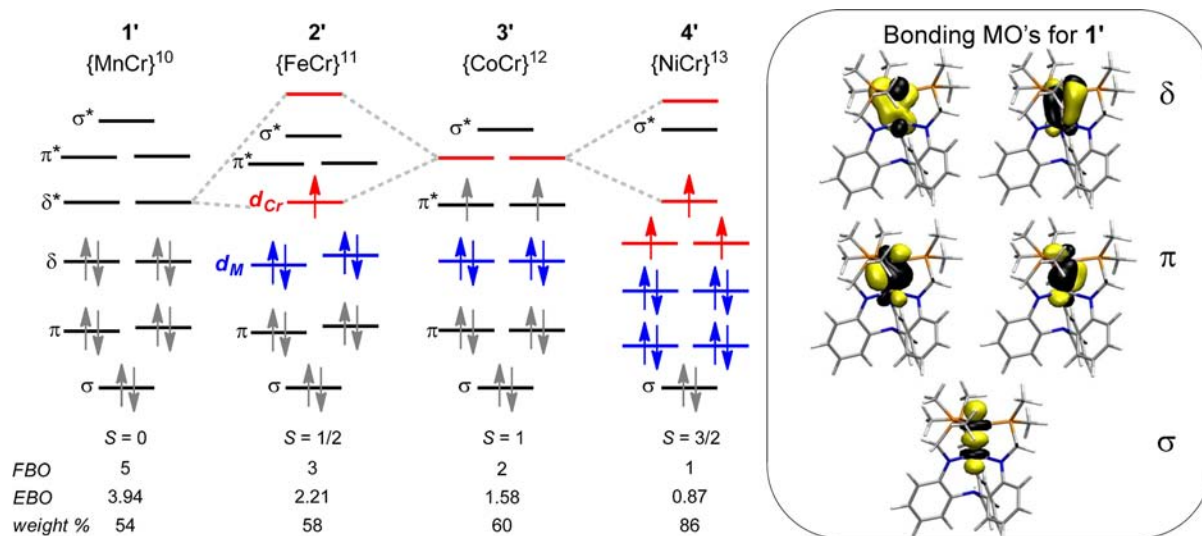


Figure 4. (Left) Qualitative MO diagrams of the d-orbital manifold for the M–Cr complexes 1'–4', based on the dominant electronic configuration (weight %) from CASSCF calculations. The {M–Cr}^{*n*} descriptor is an adaptation of the Enemark–Feltham notation, where *n* = total d-electrons.⁵⁷ The formal and effective bond orders, FBO and EBO, respectively, are shown. The d-orbitals that are localized at either the M or Cr center are indicated in blue and red, respectively. (Right) Natural bonding orbitals of σ (d_z), π (d_{xz} , d_{yz}), and δ (d_{xy} , $d_{x^2-y^2}$) symmetry for 1'.

second oxidative process at -0.18 V would correspond to the Ni(I)/Ni(0) redox couple. As mentioned above, the mononickel **5** has a nickel-based oxidation at -1.02 V. Also of relevance, an isostructural Ni–Al complex with a reverse dative bond between nickel and aluminum, i.e., Ni(0)→Al(III), has a reversible Ni(I)/Ni(0) redox couple at -0.74 V.⁵⁰ This trio of nickel species demonstrate that the Ni(I)/Ni(0) potential is determined by the identity of the supporting metal. Involvement of the nickel center in a reverse dative interaction with Al(III) induces a 300 mV change, while covalent binding of nickel to Cr(III) produces an even greater shift of over 800 mV. These bimetallic systems thus show promise for wide tuning of a metal's redox properties through careful selection of the supporting atom.^{25,30}

Theoretical Calculations. Quantum chemical studies have been conducted on the bimetallic models, **1'**, **3'**, and **4'**, where the isopropyl groups are truncated to methyls. A similar study for **2'** has been reported elsewhere.²⁴ Geometry optimizations were performed using density functional theory (DFT) for several possible spin states. For all cases, the theory confirmed the experimental ground spin states. Since it may be problematic for DFT to address the strong correlation effects expected for metal–metal bonds, we have performed complete active space self-consistent field (CASSCF) followed by second-order perturbation theory (CASPT2) calculations. CASSCF allows multiple electronic configurations to contribute to the total wavefunction, and CASPT2 recovers the dynamical correlation.^{11–13,56} Figure 4 depicts the major electronic configurations with their weights in the total wave functions (54–86%).

In the weak ligand field of trigonal coordination geometries, all five d-orbitals can potentially participate in metal–metal bonding. Hence, the d-orbitals can combine to form one σ (d_z^2), two π (d_{xz} , d_{yz}), and two δ (d_{xy} , $d_{x^2-y^2}$) bonds. In the manganese–chromium model **1'**, each of these possible bonding interactions is observed (Figure 4, right), giving a formal bond order (FBO) of 5. However, the Mn–Cr **1'** is the most multiconfigurational of this set, and partial occupation of the higher-lying orbitals, which are antibonding in nature, decreases the effective bond order (EBO) to 3.94, yielding a net quadruple bond.

For heterobimetallic complexes, the idealized 5-fold bonding breaks down further as the metals become increasingly dissimilar. As the disparity between their d-orbital energies increases (and overlap worsens), their molecular orbitals (MOs) grow increasingly polarized until they become localized at the individual metals. Indeed, for Fe–Cr **2'** and Co–Cr **3'**, the δ -symmetric d-orbitals are localized, while in Ni–Cr **4'**, both the π - and δ -symmetric d-orbitals are localized. The dominant configurations predict FBOs of 3 for **2'**, 2 for **3'**, and 1 for **4'**. Meanwhile, the EBOs are expectedly lower at 2.21, 1.58, and 0.87 for **2'**, **3'**, and **4'**, respectively. Detailed inspection of the active space orbitals can provide the d-electron counts of each metal (SI Table 7–9). The results of these analyses are consistent with the partial oxidation states: Mn(0.9)Cr(2.1) for **1'**, Fe(0.6)Cr(2.4) for **2'**, Co(0.5)Cr(2.5) for **3'**, and Ni(0.3)Cr(2.7) for **4'**. Hence, the $[\text{MCr}]^{3+}$ bimetallic cores are predicted to show a continuum of electronic distribution between the two metals, starting at M(I)Cr(II) for M = Mn and approaching M(0)Cr(III) for M = Ni.

CONCLUSION

The isolation of Mn–Cr, Co–Cr, and Ni–Cr bimetallics completes an unprecedented series of exclusively first-row metal–metal bonds. Systematic variation of the metal in this series of metal–chromium bonds demonstrates the wide tunability of bond orders (from formally quintuple to single) by exchanging the metal. An interesting periodic trend is the decrease in bond order across the period, which is primarily an effect of increasing polarity in the M–Cr bond, rather than the increasing d-electrons. This bonding paradigm will likely be applicable to other multiply bonded first-row pairs.

The observation of multiple one-electron-transfer processes in these heterobimetallics is remarkable, considering that only a single one-electron transfer was observed for the mononuclear nickel analogue. The electron-transfer chemistry of the iron–chromium, cobalt–chromium, and nickel–chromium species exemplifies the gestalt phenomenon, where the properties of the whole cannot be derived from the summation of its parts. Our future efforts are directed at exploiting the synergy of the metals within metal–metal bonds for multielectron reactivity.

ASSOCIATED CONTENT

Supporting Information

Crystallographic data in CIF format. Additional spectroscopic characterization, SQUID, CV, and computational data. This material is available free of charge via the Internet at <http://pubs.acs.org>.

AUTHOR INFORMATION

Corresponding Author

clu@umn.edu

Author Contributions

^{||}These authors contributed equally.

Notes

The authors declare no competing financial interest.

[†]Title adapted from reference 19.

ACKNOWLEDGMENTS

The authors thank Dr. Eckhard Bill (Max Planck Institute) for providing magnetic data and analyses. C.C.L. thanks Professors Doreen Leopold and Chris Thomas (Brandeis University) for helpful suggestions. This work was supported by the National Science Foundation (NSF, CHE-1254621). C.C.L. is grateful to the Alfred P. Sloan Foundation for a research fellowship. R.B.S. was supported by an NSF graduate fellowship. A.D.M. thanks the NSF-LANDO program for a summer research stipend. X-ray diffraction experiments were performed using a crystal diffractometer acquired through an NSF-MRI award (CHE-1229400) in the X-ray laboratory supervised by Dr. Victor G. Young, Jr. The computational research (N.P., S.H., and L.G.) was supported by the Office of Basic Energy Sciences, Heavy Element Chemistry program (USDOE/DE-SC002183).

REFERENCES

- (1) Cotton, F. A. *J. Chem. Educ.* **1983**, *60*, 713.
- (2) *Multiple Bonds Between Metal Atoms*; Cotton, F. A., Murillo, C. A., Walton, R. A., Eds.; Springer Science: New York, 2005.
- (3) Cotton, F. A.; Curtis, N. F.; Harris, C. B.; Johnson, B. F. G.; Lippard, S. J.; Mague, J. T.; Robinson, W. R.; Wood, J. S. *Science* **1964**, *145*, 1305.
- (4) Cotton, F. A.; Curtis, N. F.; Johnson, B. F. G.; Robinson, W. R. *Inorg. Chem.* **1965**, *4*, 326.

- (5) Cotton, F. A.; Harris, C. B. *Inorg. Chem.* **1965**, *4*, 330.
- (6) Nguyen, T.; Sutton, A. D.; Brynda, M.; Fettinger, J. C.; Long, G. J.; Power, P. P. *Science* **2005**, *310*, 844.
- (7) Hsu, C.-W.; Yu, J.-S. K.; Yen, C.-H.; Lee, G.-H.; Wang, Y.; Tsai, Y.-C. *Angew. Chem., Int. Ed.* **2008**, *47*, 9933.
- (8) Tsai, Y.-C.; Hsu, C.-W.; Yu, J.-S. K.; Lee, G.-H.; Wang, Y.; Kuo, T.-S. *Angew. Chem., Int. Ed.* **2008**, *47*, 7250.
- (9) Noor, A.; Glatz, G.; Müller, R.; Kaupp, M.; Demeshko, S.; Kempe, R. *Nat. Chem.* **2009**, *1*, 322.
- (10) Kreisel, K. A.; Yap, G. P. A.; Dmitrenko, O.; Landis, C. R.; Theopold, K. H. *J. Am. Chem. Soc.* **2007**, *129*, 14162.
- (11) Brynda, M.; Gagliardi, L.; Widmark, P.-O.; Power, P. P.; Roos, B. O. *Angew. Chem., Int. Ed.* **2006**, *45*, 3804.
- (12) La Macchia, G.; Aquilante, F.; Veryazov, V.; Roos, B. O.; Gagliardi, L. *Inorg. Chem.* **2008**, *47*, 11455.
- (13) La Macchia, G.; Li Manni, G.; Todorova, T. K.; Brynda, M.; Aquilante, F.; Roos, B. O.; Gagliardi, L. *Inorg. Chem.* **2010**, *49*, 5216.
- (14) Kurokawa, Y. I.; Nakao, Y.; Sakaki, S. *J. Phys. Chem. A* **2009**, *113*, 3202.
- (15) Collman, J. P.; Boulatov, R. *Angew. Chem., Int. Ed.* **2002**, *41*, 3948.
- (16) Greenwood, B. P.; Rowe, G. T.; Chen, C.-H.; Foxman, B. M.; Thomas, C. M. *J. Am. Chem. Soc.* **2010**, *132*, 44.
- (17) Slaughter, L. M.; Wolczanski, P. T. *Chem. Commun.* **1997**, 2109.
- (18) Garner, C. D.; Senior, R. G.; King, T. J. *J. Am. Chem. Soc.* **1976**, *98*, 3526.
- (19) Collman, J. P.; Barnes, C. E.; Woo, L. K. *Proc. Natl. Acad. Sci. U.S.A.* **1983**, *80*, 7684.
- (20) Weltner, W., Jr.; Van Zee, R. J. *Annu. Rev. Phys. Chem.* **1984**, *35*, 291.
- (21) Morse, M. D. *Chem. Rev.* **1986**, *86*, 1049.
- (22) Spain, E. M.; Morse, M. D. *J. Phys. Chem.* **1992**, *96*, 2479.
- (23) Gutsev, G. L.; Mochena, M. D.; Jena, P.; Bauschlicher, C. W., Jr.; Partridge, H., III. *J. Chem. Phys.* **2004**, *121*, 6785.
- (24) Rudd, P. A.; Liu, S.; Planas, N.; Bill, E.; Gagliardi, L.; Lu, C. C. *Angew. Chem., Int. Ed.* **2013**, *52*, 4449.
- (25) Kuppuswamy, S.; Powers, T. M.; Krogman, J. P.; Bezpalko, M. W.; Foxman, B. M.; Thomas, C. M. *Chem. Sci.* **2013**, *4*, 3557.
- (26) For gas-phase examples, see references 26–28. Cheeseman, M.; Van Zee, R. J.; Flanagan, H. L.; Weltner, W., Jr. *J. Chem. Phys.* **1990**, *92*, 1553.
- (27) Nagarathna, H. M.; Montano, P. A.; Naik, V. M. *J. Am. Chem. Soc.* **1983**, *105*, 2938.
- (28) Lu, H.; Zhao, B.; Lombardi, J. R. *Chem. Phys. Lett.* **2003**, *376*, 49.
- (29) Nippe, M.; Goodman, S. M.; Fry, C. G.; Berry, J. F. *J. Am. Chem. Soc.* **2011**, *133*, 2856.
- (30) Greenwood, B. P.; Forman, S. I.; Rowe, G. T.; Chen, C.-H.; Foxman, B. M.; Thomas, C. M. *Inorg. Chem.* **2009**, *48*, 6251.
- (31) Weast, R. C.; Astle, M. J. *CRC Handbook of Chemistry and Physics*; CRC Press Inc.: Boca Raton, FL, 1979.
- (32) Bill, E. *JulX Version 141*; available from: http://ewww.mpi-muelheim.mpg.de/bac/logins/bill/julX_en.php.
- (33) Spek, A. L. *Acta Crystallogr.* **2009**, *D65*, 148.
- (34) Perdew, J. P.; Burke, K.; Ernzerhof, M. *Phys. Rev. Lett.* **1996**, *77*, 3865.
- (35) Ahlrichs, R.; Bär, M.; Häser, M.; Horn, H.; Kölmel, C. *Chem. Phys. Lett.* **1989**, *162*, 165.
- (36) *TURBOMOLE V6.4, A Development of University of Karlsruhe and Forschungszentrum Karlsruhe GmbH*; TURBOMOLE GmbH: Karlsruhe, 1989–2007; available from <http://www.turbomole.com>.
- (37) Eichkorn, K.; Treutler, O.; Öhm, H.; Häser, M.; Ahlrichs, R. *Chem. Phys. Lett.* **1995**, *240*, 283.
- (38) Roos, B. O.; Taylor, P. R.; Siegbahn, P. E. M. *Chem. Phys.* **1980**, *48*, 157.
- (39) Andersson, K.; Malmqvist, P.-Å.; Roos, B. O.; Sadlej, A. J.; Wolinski, K. *J. Phys. Chem.* **1990**, *94*, 5483.
- (40) Andersson, K.; Malmqvist, P.-Å.; Roos, B. O. *J. Chem. Phys.* **1992**, *96*, 1218.
- (41) Aquilante, F.; De Vico, L.; Ferré, N.; Ghigo, G.; Malmqvist, P.-Å.; Pedersen, T.; Neogrády, P.; Pitoňák, M.; Reiher, M.; Roos, B. O.; Serrano-Andrés, L.; Urban, M.; Veryazov, V.; Lindh, R. *J. Comput. Chem.* **2010**, *31*, 224.
- (42) Douglas, M.; Kroll, N. M. *Ann. Phys.* **1974**, *82*, 89.
- (43) Hess, B. A. *Phys. Rev. A* **1986**, *33*, 3742.
- (44) Roos, B. O.; Lindh, R.; Malmqvist, P.-Å.; Veryazov, V.; Widmark, P.-O. *J. Phys. Chem. A* **2004**, *108*, 2851.
- (45) Roos, B. O.; Lindh, R.; Malmqvist, P.-Å.; Veryazov, V.; Widmark, P.-O. *J. Phys. Chem. A* **2005**, *109*, 6575.
- (46) Aquilante, F.; Pedersen, T. B.; Lindh, R. *J. Chem. Phys.* **2007**, *126*, 194106.
- (47) Aquilante, F.; Pedersen, T. B.; Lindh, R.; Roos, B. O.; de Merás, A. S.; Koch, H. *J. Chem. Phys.* **2008**, *129*, 24113.
- (48) Aquilante, F.; Malmqvist, P.-Å.; Pedersen, T. B.; Ghosh, A.; Roos, B. O. *J. Chem. Theory Comput.* **2008**, *4*, 694.
- (49) Gagliardi, L.; Lindh, R.; Karlström, G. *J. Chem. Phys.* **2004**, *121*, 4494.
- (50) Rudd, P. A.; Liu, S.; Gagliardi, L.; Young, V. G.; Lu, C. C. *J. Am. Chem. Soc.* **2011**, *133*, 20724.
- (51) McGlinchey, M. J. *Inorg. Chem.* **1980**, *19*, 1392.
- (52) San Filippo, J., Jr. *Inorg. Chem.* **1972**, *11*, 3140.
- (53) Allen, F. *Acta Crystallogr., Sect. B* **2002**, *58*, 380.
- (54) Turov, Y.; Berry, J. F. *Dalton Trans.* **2012**, *41*, 8153.
- (55) Pauling, L. *The Nature of the Chemical Bond*, 3rd ed.; Cornell University Press: Ithaca, NY, 1960.
- (56) Brynda, M.; Gagliardi, L.; Roos, B. O. *Chem. Phys. Lett.* **2009**, *471*, 1.
- (57) Enemark, J. H.; Feltham, R. D. *Coord. Chem. Rev.* **1974**, *13*, 339.